The Effect of Rocker on Ice Friction in Short-Track Speed Skating

Van Gelderen, A. (4207734) a.vangelderen@student.tudelft.nl
Thesis Report, Delft University of Technology, MSc Mechanical Engineering - BioMechanical Design
Supervisor: Prof. Dr. F.C.T. Van der Helm

***Abstract*— Short-track speed skates are prepared with rocker to improve cornering behavior. However, rocker also has a negative impact on ice friction. As there is currently no scientific theory for selecting optimal rocker profiles, skaters have to rely on personal experience. There is a lack of experimental data available in literature to validate current hypotheses for ice friction. A setup was designed to measure ice friction of an upright skate with varying rocker profiles and normal loads. The experiment was conducted on the artificial ice rink at Thialf, Heerenveen. A sled fitted with two parallel blades was towed at a constant speed of approximately 1.5 ms^{-1}. A force transducer was used to measure friction forces on the sled. Short-track and long-track blades with representative rocker radii were tested. A strong correlation was found between rocker radius and ice friction. Friction forces were found to be on average greater by a factor of 1.868($\pm$0.050) for blades with rocker radius of 10 m compared to 21 m. The results further show high repeatability between tests. This study demonstrates the impact of rocker on ice friction in speed skating. Further research is needed to establish a valid theory for optimal rocker selection. This test method can be used in the future to include different variables, such as ice temperature, sliding speed or blade inclination angle. The method is not limited to short-track speed skating, but can be applied to other disciplines.**

I. Introduction

A. Ice Friction in Speed Skating

Ice skating is an efficient mode of human-powered transport, which exploits the extraordinarily low friction coefficient of ice. A significant amount of energy is still lost to ice friction in speed skating. De Koning et al. [1] estimated that approximately 25% of a skater's frictional losses can be attributed to ice friction when skating at a speed of 10 ms^{-1}. Skaters try to minimize ice friction with the setup of their skates. An important blade parameter in short track speed skating is rocker. Rocker refers to the curvature ground into a skate's blade, as shown in Fig. 1a, and is quantified by its radius of curvature r_{rocker}. Rocker is used to improve a skate's cornering behavior. Ice friction tends to increase however with smaller rocker radii. This is a generally accepted rule among skaters. A trade-off therefore has to be made between ice friction and cornering performance. Rocker profiles are currently chosen with the primary focus on cornering performance. A scientific theory for selecting optimal rocker profiles does not currently exist. Instead, this choice is mostly subjective and relies on the experience of skaters and coaches. This makes skate setup choices difficult for beginning skaters. A better understanding of the effects of rocker on ice friction in speed skating is needed for establishing a scientific theory.

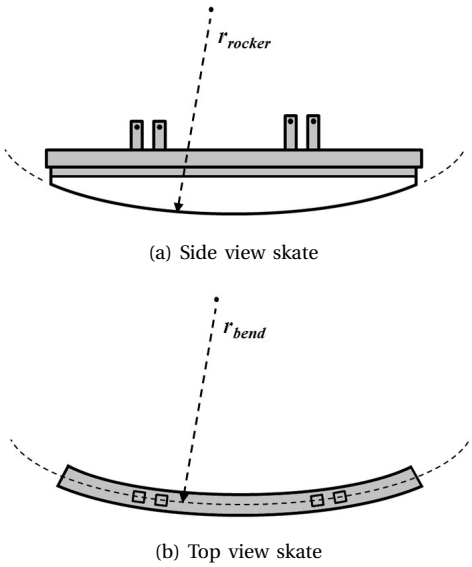

(a) Side view skate

(b) Top view skate

Fig. 1: Exaggerated examples of rocker radius r_{rocker} and bend radius r_{bend}.

B. Rocker and Bend

Rocker is essential for any ice skate in order to steer. A rockered blade makes contact with the ice

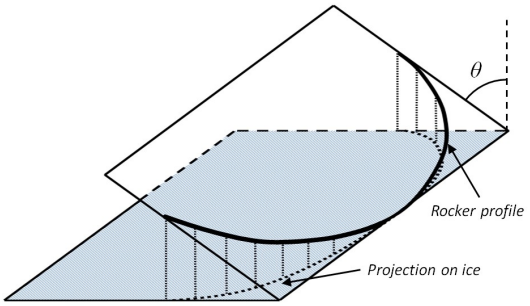

Fig. 2: Rocker Projection

on a shorter area. This allows the skate to pivot and improves manoeuvrability. The smaller contact area results in higher pressure on the ice. As a result the blade cuts deeper tracks, thereby losing energy to plastic deformation of the ice. When cornering the blade makes contact with the ice at an incline θ, as shown in Fig.2. The projection of the rocker profile on the ice is generally assumed to describe a skates natural path. Its radius of curvature is called the resultant radius and ideally matches to the corner radius of the track. In addition to rocker, short-track speed skaters bend their blades with the direction of the corners on the track. Similar to rocker, bend is also quantified by radius of curvature r_{bend}, as shown in Fig.1b. Bend is used to increase the contact area of the blade with the ice during cornering, when ice reaction forces are highest. This reduces pressure on the ice and prevents the ice from breaking. The combination of rocker and bend eventually determines the resultant radius of a skate.

C. Friction

Friction is the resistance against relative motion between surfaces in contact with each other. Friction can be expressed as the force F_f in Eq. (1), where μ is the coefficient of friction and F_N is the normal force between the surfaces.

$$F_f = \mu F_N \tag{1}$$

Ice has a remarkably low coefficient of friction compared to most other solids. This is caused by a thin layer of water that is present on the surface of ice under most conditions. This water layer acts as a lubricant in the skate-ice contact zone. The thickness of the water layer is generally considered an important factor in determining ice friction in skating [2]. The friction coefficient of ice can be interpreted as the sum of three parts: Coulomb friction, viscous friction and ploughing friction. This can be expressed as Eq.(2), where μ_c, μ_v, and μ_p are the coefficients of Coulomb-, viscous-, and ploughing friction, respectively.

$$\mu = \mu_c + \mu_v + \mu_p \tag{2}$$

Coulomb friction is also known as dry friction and occurs in solid-solid contact between surfaces. Friction forces arise from the shearing of adhesive bonds that form between opposing surface asperities. As surfaces theoretically only make contact in three points, the apparent area of contact cannot be used to describe Coulomb friction. The actual area of contact between asperities must be used to determine shear forces. According to Bowden [3] the actual contact area depends solely on contact pressure and hardness of the softer material. The coefficient μ_c can then be expressed as Eq.(3), with τ the shear strength of the adhesions and H the hardness of the softer material.

$$\mu_c = \frac{\tau}{H} \tag{3}$$

Coulomb friction is defined by three empirical laws, which state that Coulomb friction is:

- Independent of apparent contact area
- Directly proportional to normal force
- Independent of sliding speed

Viscous friction arises in lubricated contact. A lubricant in the contact zone absorbs part of the pressure between the surfaces. This reduces Coulomb friction by reducing solid-solid contact between asperities on opposing surfaces. The relative motion between surfaces induces a flow in the lubricant, referred to as Couette flow. A shear stress is imposed on the lubricant due to its viscosity, which results in viscous friction. As opposed to Coulomb friction, viscous friction is dependent on sliding speed. Its coefficient μ_v is expressed as Eq.(4), where η is lubricant viscosity, v is sliding speed and h is lubrication layer thickness.

$$\mu_v = \frac{\eta v}{hH} \tag{4}$$

Ploughing friction refers to the blade carving a groove through the ice. This results in the characteristic skate tracks. The geometry of the ice-blade contact is shown in Fig.3. The contribution of ploughing to friction depends on the hardness of the

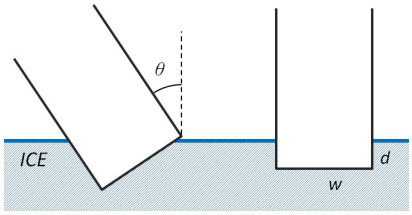

(a) Rear view skate

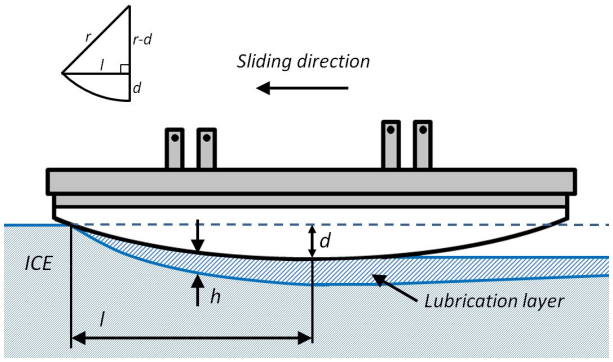

(b) Side view skate

Fig. 3: Contact Geometry Blade. l) Length of blade-ice contact; h) Lubrication layer thickness; d) Penetration depth; w) Blade width; θ) Inclination angle. Inset: r) Rocker radius

ice[4] and the cross-sectional area of the groove A_c, as expressed in Eq.(5).

$$F_p = HA_c \tag{5}$$

An upright speed skating blade has a square A_c, as it is sharpened flat at the bottom, shown in Fig.3a. The area can be expressed as Eq.(6), where d is the penetration depth and w the width of the blade. A standard blade width of 1.1 mm is used in speed skating.

$$A_c = wd \tag{6}$$

To determine d we must consider the equilibrium between the normal force and the ice reaction force. The ice reaction force is limited to the hardness H over the area of contact. This must be greater than or equal to F_N to resist further indentation of the blade, as shown in Eq.(7), where l is the blade-ice contact length.

$$F_N \leq lwH \tag{7}$$

A side view of the contact geometry of a sliding blade is shown in Fig.3b. A forward moving skate makes contact with ice up until its lowest point,

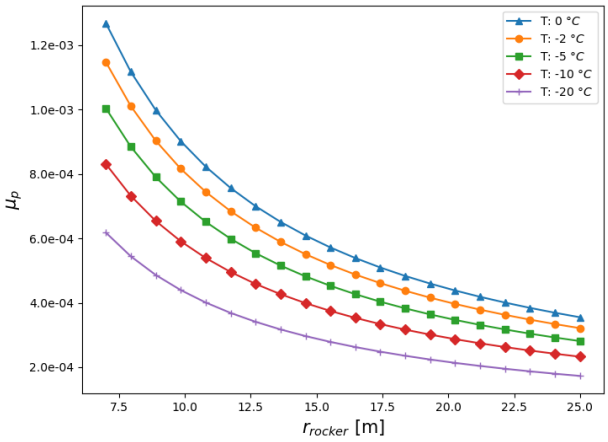

Fig. 4: Estimated ploughing friction coefficient

after which the blade curves away from the created groove. As the blade penetrates further into the ice, l increases due to the curvature of the blade. The inset in Fig.3b shows the simple geometry that gives the relation between l, r_{rocker}, and d as Eq.(8).

$$d = r_{rocker} - \sqrt{r_{rocker}^2 - l^2} \tag{8}$$

This finally results in an expression for coefficient μ_p give in Eq.(9).

$$\mu_p = \left(r_{rocker} - \sqrt{r_{rocker}^2 - (\frac{F_N}{wH})^2} \right) \frac{wH}{F_N} \tag{9}$$

Liefferink et al.[4] report a linear dependency of ice hardness on ice temperature T Eq.(10).

$$H = (-1.01T + 19.2) \times 10^6 \tag{10}$$

From Eq.(9) and (10) follows Fig.4, showing mu_p for different r_{rocker} values and temperature. F_N = used is 750 N and a width w of 2.2 mm is used to represent two blades. The estimated values show a decrease in μ_p of 2.9×10^{-4} from an r_{rocker} of 10 m to 21 m at T=−10 celsius. This is less than 10% of the total expected ice friction coefficient. Research by Liefferink et al.[4] shows a strong dependency of ice hardness on sliding speed. They also suggest ice to be non-isotropic with respect to hardness and to respond differently to variations in sliding speed compared to indentation speed.

D. Literature research

A number of articles have been published on ice friction theory in speed skating. Lozowski et al.[5][6] and Makkonen and Tikanmaki [7] have made promising efforts towards establishing analytic models for ice friction, but have insufficient validation through experimental evidence. These publications highlight the complexity of ice friction physics. The FAST 2.0(i) model by Lozowski describes ice friction in the absence of Coulomb friction. In this model the lubrication layer thickness h determines viscous friction. The model additionally includes ploughing friction. It considers melting of ice due to friction, heat conduction into the ice and squeeze flow in predicting h. Makkonen and Tikanmaki approach ice friction by solving the thermodynamic balance in the blade-ice contact, which eliminates the need for calculating h. This model does not currently include ploughing friction however.

One single experiment by De Koning et al. [1] was found in literature on testing ice friction in an actual speed skating context. The resulting ice friction coefficients can be seen against temperature and velocity in Fig. 5. The experiment was conducted with instrumented skates measuring ice friction forces in horizontal direction and normal forces in vertical direction using strain gauges. This introduces the risk of cross-talk. Cross-talk is especially problematic for ice friction forces, which are approximately 0.005 times the magnitude of normal forces. The reported cross-talk by De Koning ranges from 0.03 to 0.08%, which is significant. The experiment was done with a single subject skating on three different artificial ice rinks. The scientific relevance of the experiment is limited on account of the extremely small sample size used (N=1). Skating technique and physical traits of the skater are two major confounding variables in this research which have not been properly addressed. Effects caused by the use of a non-standard skate must also be considered a possible influence on the results. The results from De Koning et al. do however serve as the sole source of validation for current ice friction models. They give insights into approximate values and behaviors of ice friction coefficients in speed skating.

Other experiments have been performed in laboratory settings [8][9] and with slider models on ice rinks [10][11]. No experiments were found that include the effects of rocker on ice friction. Furthermore, in the specific context of short-track speed skating no experiments on ice friction were found. It was concluded that linearly guided slider models offer a good solution for testing ice friction in an objective, controllable and reliable manner. It offers the freedom to use actual ice rinks and skate blades to guarantee realistic conditions with sufficient control over remaining variables.

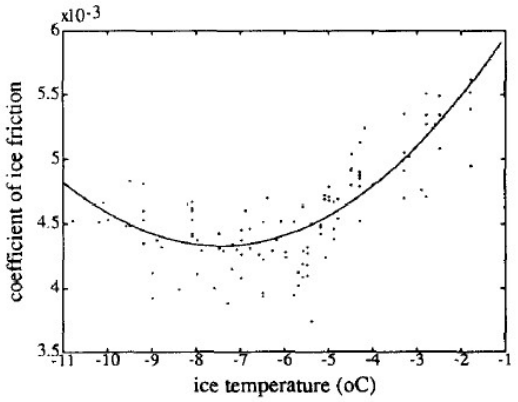

(a) Friction Coefficients against Ice Temperature

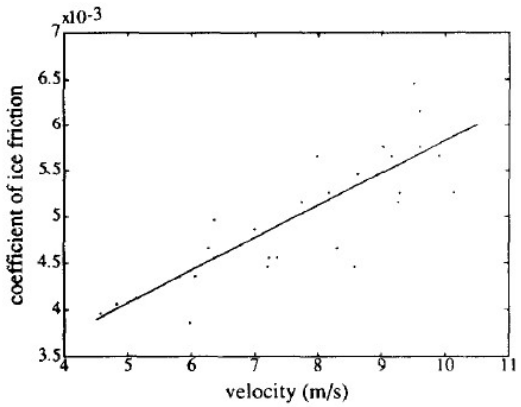

(b) Friction Coefficients against Velocity

Fig. 5: Ice friction coefficients measured by De Koning et al. [1]

E. Problem Statement and Research Goal

There is currently no validated theory for ice friction in speed skating that includes the influence of rocker, caused by a lack of available experimental data. Short-track skaters are forced to rely on subjective feedback and experience in the setup of their blades. The choice and application of rocker and bend profiles appears to be closer to an art form than a science currently. This poses the question whether or not skaters are unknowingly sacrificing more sliding efficiency than necessary. A better understanding of the impact of rocker on ice friction is needed to

improve skate setup decisions. Therefore the goal of this research is to study the following: *What is the impact of rocker on ice friction in short-track speed skating?*

II. Method

A. Measurement setup

The measurement setup consists of a sled with two parallel skates, a load cell, a towing cart, two wheels relaying position and orientation feedback and a microcontroller for data collection, as shown schematically in Fig. 6. The device measures reaction forces between the sled and the cart. It simultaneously measures the position of the cart in time. The cart was introduced to separate the position feedback device from the sled. This separation ensures that friction forces resulting from position feedback do not interfere with the ice friction measurements. The rigid connection between cart and sled allows measurement of both tension and compression. The cart was accelerated via a rope connected to the front of the cart, indicated by propulsion force F_P. Friction force F_f can be deduced from the force and position signals. Normal force F_N is known and can be used to determine the friction coefficient.

B. Connection assembly

Reaction forces on the sled propagate through a connection assembly from the sled (8.b), through the load cell (1), to the cart (8.a). This assembly includes threaded rods on both sides of the load cell. These attach to tapped holes present on the load cell. The assembly exits the protective casing through a small hole, with sufficient margin to avoid contact. The threaded rod transitions to a round steel bar with a diameter of 8 mm (transition not visible behind wheel (2) in figure). A linear bearing (3) constrains the assembly to maintain a proper alignment with 8.a. The bearing can freely rotate in the horizontal plane, to avoid internal friction from improper alignment. Furthermore, it allows axial translation of the assembly. A ball-and-socket joint connects the bar to a damper (4). This joint allows steering of the cart, without subjecting the load cell to any damaging bending moments. The damper serves to protect the load cell from overloading due to peak forces in unexpected events of rapid deceleration. The damper at rest is in full extension. Its spring is preloaded, such that it can be considered a rigid object in normal operation. Finally, a second round steel bar extends from the damper to the sled (8.b). The bar is constrained to always be parallel with the sliding direction of the sled.

C. Blades

The experiment was conducted using a pair of short-track (ST) blades and a pair of long-track (LT) blades, shown in Fig.7. The ST and LT blades are prepared with an average r_{rocker} of approximately 10 m and 21 m, respectively. The rocker profiles were measured using a Marchese Racing blade gauge, a three-point radius measurement device with a length of 10 cm. The average rocker radii of the blade pairs is measured in 5 points along the blade, as shown in Table I. Each r_{rocker} describes a 10 cm section of blade, centered about the given position. The positions are described relative to the rocker point of the blade, which indicates the lowest point on the blade in a horizontal position. The lengths of the ST and LT blades are respectively 43.0 cm and 40.5 cm, and have a width of 1.1 mm. The blades were prepared with rocker by a professional and surface treated by hand with a whetstone.

TABLE I: Rocker radius profiles

	Long Track		Short Track	
Pos.[1] (m)	r_{rocker} (m)	(±SD)	r_{rocker} (m)	(±SD)
-0.12	19.7	(0.11)	8.5	(0.12)
-0.06	20.5	(0.09)	9.9	(0.09)
0	21.4	(0.03)	10.1	(0.07)
0.06	20.5	(0.10)	8.8	(0.12)
0.12	16.7	(0.15)	6.9	(0.17)

[1] Position relative to the rocker point of the blade, with positive values to the front.

D. Sled

The sled (6) consists of a skate-sharpening jig fitted with two blades, as shown in Fig. 8. The jig ensures parallel alignment and upright blade positioning. The jig tightens on the blades along its entire length, locking them securely and vertically in place. The jig is placed inverted on the ice and up to three 25 kg weight plates (5) are stacked on top, centered horizontally above the rocker point of the blades around a column (7). The isolated sled has a mass of 3.288 kg, without ballast. The mass of the ST and LT blade-pairs are 0.719 kg and 0.876 kg, respectively.

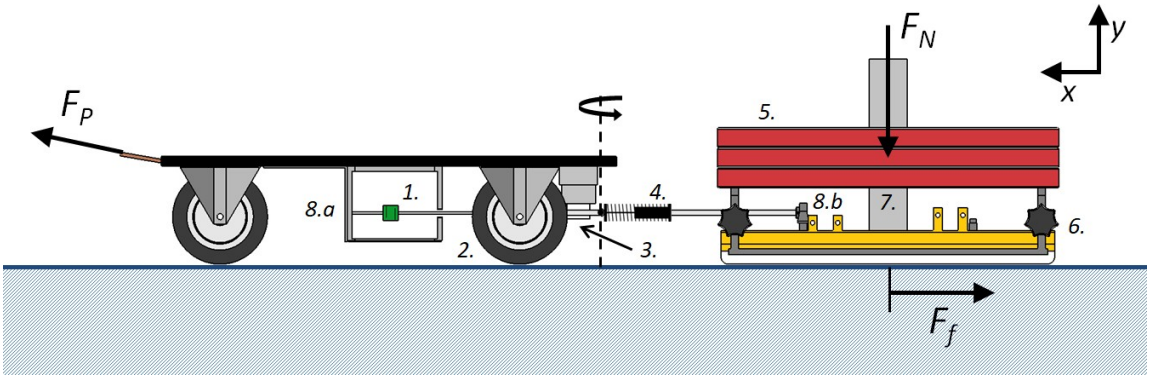

Fig. 6: Measurement Setup. 1) Load cell (green) in protective casing (cross-section); 2) Two wheels with position feedback; 3) Linear bearing; 4) Damper with ball-and-socket joint (indicated by dotted line); 5) Weight plates; 6) Skate sharpening jig (grey) and skates (yellow); 7) Weight plate alignment cylinder; 8) Force propagation from the cart in 8.a to the jig in 8.b.

Fig. 7: Skate blades used in tests. Left: Long-Track. Right: Short-Track

E. Cart

A cart was used for towing the sled, providing position feedback and housing the load cell and electronics. The cart consists of an aluminum bread-board on two rigid caster wheels and a swivel wheel centred at the front. The axles of the rear wheels are attached to EC11 rotary encoders, as shown in Fig.9. These enable position and orientation feedback with 20 mm resolution per wheel. Proper traction of the wheels on the ice is achieved through the use of stainless steel staples on the wheel's driving surface. The load cell is attached underneath the breadboard and housed in an isolated casing. The cart further serves to carry the microcomputer and the battery pack. The cart is propelled manually with a rope and operated at walking pace.

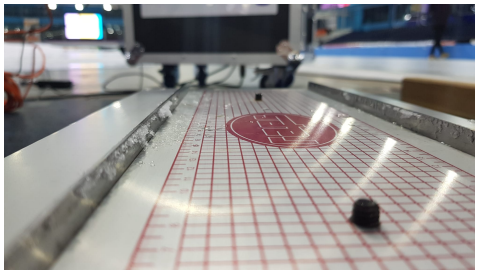

(a) Bottom view sled

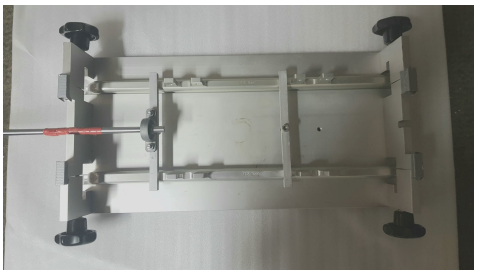

(b) Top view sled

Fig. 8: Sled pictures

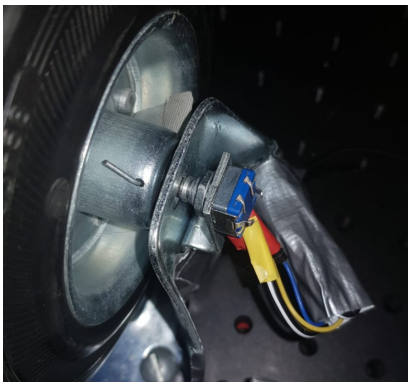

Fig. 9: Rotary encoder attached to wheel axle

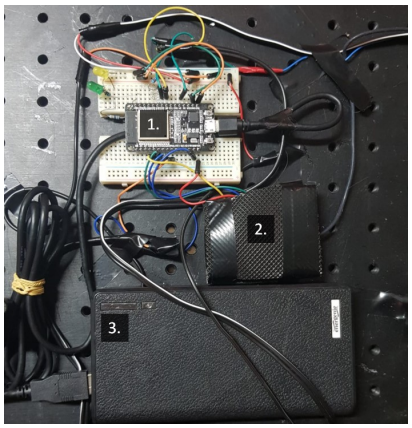

Fig. 10: Electronics. 1) ESP32 microcontroller; 2) HX711 A/D converter in isolation foam; 3) 5V battery pack power supply

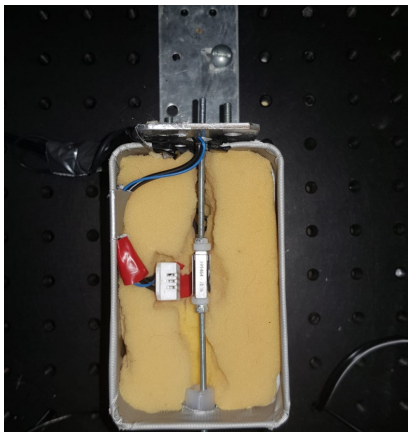

Fig. 11: Load cell (centre) with temperature sensor (left) in protective case. Protective case shown without foam-lined lid.

F. Load cell and data acquisition

A 45N Futek LSB200 miniature load cell was used to measure friction force. The load cell signal was amplified and 24 bit A/D converted by an HX711 load cell amplifier before being fed into a micro-controller unit (MCU). The MCU model used is an ESP32 DevKit v1, powered by a 5 V battery pack. The electronic layout is shown in Fig.10. Its WiFi module allows communication with a PC through a WiFi client-server networking protocol, enabling remote timing control and wireless data transmission. The registered data is initially stored in internal memory and subsequently transmitted to the PC upon test completion. To correct for effects of temperature and humidity on measurements the load cell is placed in a foam-lined casing along with a DHT22 temperature and humidity sensor, as shown in Fig.11.

G. Measurements

The experiments were performed on a straight section of the 333 m track at Thialf in Heerenveen, The Netherlands. The track was not in use during times of testing by any of the training groups. The chemical make-up and creation process of the ice is identical to that of the short track rink at Thialf, according to the ice maintenance crew. Prior to each test session the ice was prepared with a Zamboni ice resurfacer. Tests were scheduled in a random chronological order to reduce bias resulting from time since resurfacing. Each blade-type and weight combination was tested on multiple separate occasions. The setup was placed on the ice a minimum of 10 minutes prior any test run to allow temperatures to settle.

H. Data analysis

The data is recorded with a sampling frequency of 50 Hz and passed through a low-pass, fourth order Butterworth filter with a 12 Hz cut-off frequency. The position data is averaged over the two wheels and smoothed with a Savitzky-Golay filter with a 1.0 s window. Linear and angular velocity of the cart are found by differentiation of the position signal with respect to time. A second differentiation step on the signal is done to acquire the acceleration of the cart in time. The duration of a full test run is 50 seconds. In periods of high acceleration or rotation the force data does not accurately reflect ice friction. Data was selected for analysis based on absolute threshold values for acceleration (a) and angular velocity (ω). Data points were discarded if averaged over a 1.5 s symmetric time window the following condition holds: ($|a| > 0.08\,\mathrm{m\,s^{-2}}$) OR ($|\omega| > 0.1\,\mathrm{rad\,s^{-1}}$).

III. Results

A. Test data example

An example of the measured friction force from a single test run is shown in Fig. 12, along with the accompanying speed and orientation. Three phases can be identified in the graphs, i.e. acceleration (*I*), constant speed (*II*) and deceleration & return (*III*). Since the force is measured from a non-inertial reference frame it is affected by d'Alembert forces during acceleration of the system. According to Newton's second law of motion, as shown in Eq.(11), the d'Alembert forces are derived from the measured

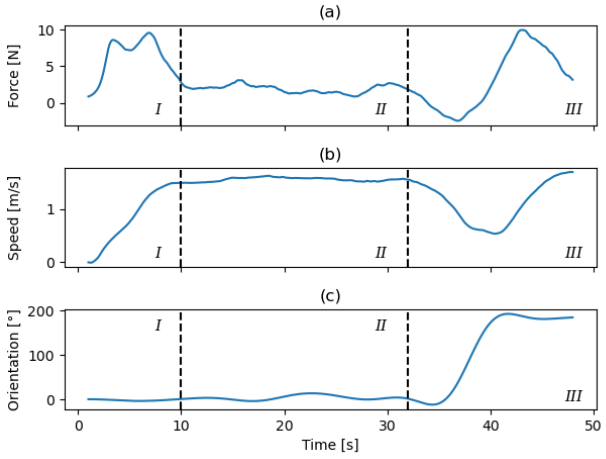

Fig. 12: Example measurement data; mass= 25 kg; blade type= LT. Phases: *I*-acceleration, *II*-constant speed, *III*-deceleration & return.

acceleration and mass of the system. This is represented in Fig. 12.a, phase *I*, by a high sustained force during steady acceleration in Fig. 12.b. Similarly, negative d'Alembert forces appear in phase *III*. Due to the magnitude of the d'Alembert forces relative to the frictional forces only data from phase *II* is used for analysis.

$$F = ma \tag{11}$$

The remaining force signal still contains noise due to d'Alembert forces from minor speed fluctuations. The force signal is fitted to the acceleration noise using linear least squares regression, shown in Fig. 14. The resulting equations are shown in the subfigures in the form $F = F_f + ma$, where m is mass and a is acceleration. The y-intercept coefficient represents the acceleration-adjusted friction force and m the 'apparent' mass of the sled and ballast. The fits all show a clear linear relationship with a high R-squared value, indicating a good fit. The data appears to be normally distributed about the baseline. The spread of the data about the baseline is quantified as the root mean square error (rmse). The rmse is quite substantial, but with a sufficiently large sample size statistically significant results can be achieved. The apparent masses consistently show lower values than the expected combined mass of the sled and the ballast.

B. All Data

The resulting ice friction forces of the two blade types are shown in Fig. 13a, with the corresponding

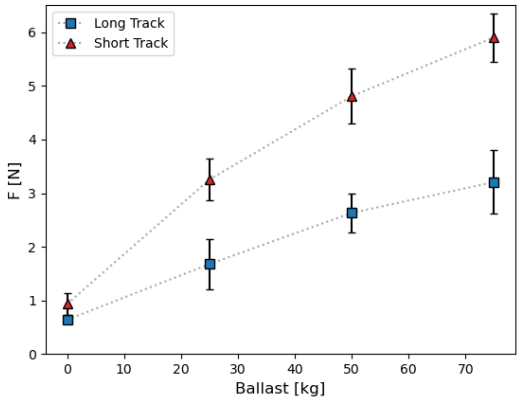

(a) Ice friction force

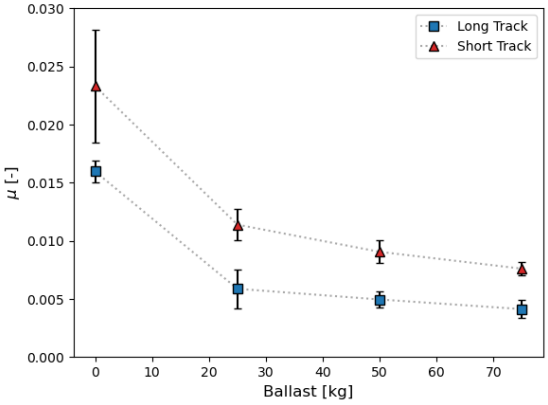

(b) Ice friction coefficients

Fig. 13: Scatter plots of measured ice friction force and corresponding friction coefficients

friction coefficients μ shown in Fig. 13b. The different blade types are clearly distinguishable in the data, with non-overlapping error bars. Ice friction forces are shown to increase with normal force. The relationship appears to be non-linear, indicated by the effect tapering off with increasing normal force. This is reflected by the ice friction coefficients, which decrease with normal force. The data further indicate distinctly higher friction coefficients for the ST blades relative to the LT blades. ST blade friction forces are registered to be higher on average by a factor α of 1.868 ($\pm$0.050), for data points with ballast values of at least 25 kg. No speed dependence on friction coefficients could be determined from the results.

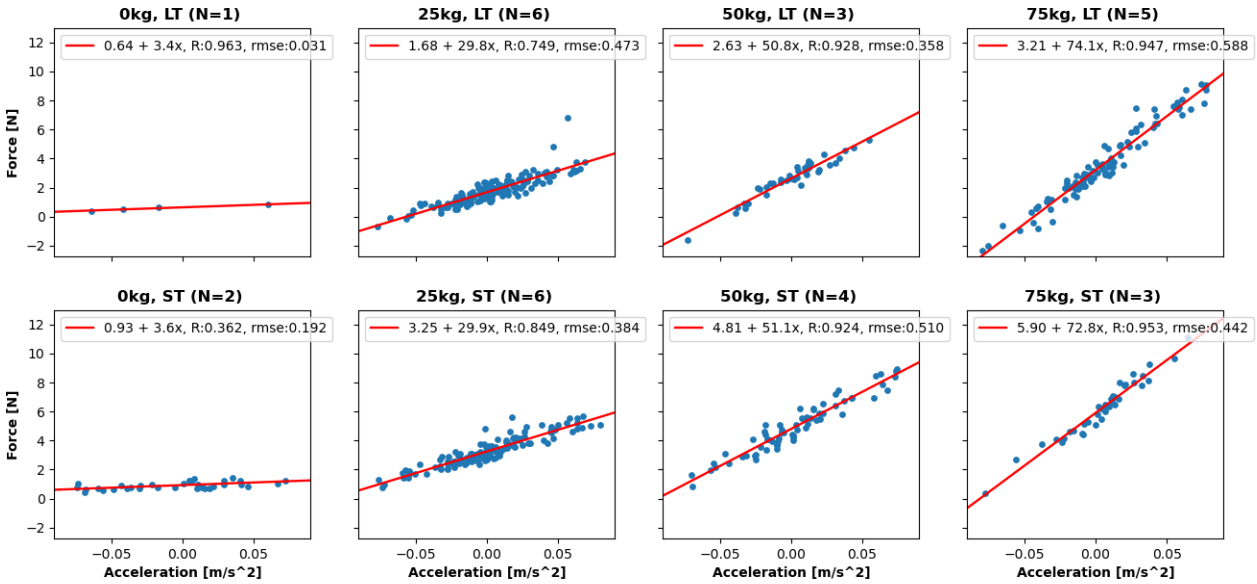

Fig. 14: Force data. A dot represents a data segment with $\Delta t = 1.5s$, $|a| < 0.08 m/s^2$ and $v > 1 m/s$.

IV. Discussion

A. Impact rocker on ice friction

The results shown in Fig.13b consistently show significantly higher friction coefficients for the ST blades relative to the LT blades. The impact of the factor α of 1.868 found in Sec. III-B can be shown by calculating the resulting speed difference. An example ice friction calculation is given by De Koning et al. [1], to which α can be applied. The power lost to ice friction can be expressed as Eq.(12), where μ is the friction coefficient, F_N is normal force and v is skating speed.

$$P_{Ice} = \mu F_N v \tag{12}$$

The example by De Koning was calculated for a μ of 0.005, a normal force F_N of 750 N and a speed v of 10 m s^{-1}. The resulting P_{Ice} accounts to 37.5 W. For the comparison we take this value to represent LT blades. Then we can recalculate P_{Ice} for ST blades in the same situation by increasing μ by the factor α. For ST blades P_{Ice} then accounts to 70.1 W. De Koning estimated that ice friction is responsible for approximately 25% of total friction at a speed of 10 m s^{-1}, as previously stated in Sec.I-A. This ice friction increase would represent a total friction increase of 21.7%.

Using the found ice friction increase and assuming speed-independent friction and drag coefficients, the effect on speed for this skater can be roughly estimated. The total power lost to friction includes the power lost to aerodynamic drag, expressed in Eq.(13).

$$P_{Air} = 0.5 \rho A C_D v^3 \tag{13}$$

We can simplify the expression by reducing the constant terms $0.5 \rho A C_D$ to a single constant D. This results in the equation for total power lost shown in Eq.(14).

$$P = \mu F_N v + D v^3 \tag{14}$$

The resulting speed $\bar{v}$ for ST blades can be found by solving eq. (15). The left hand side represents LT blades and the right hand side ST blades. This results in a speed reached for the same skater on ST blades of 9.14 m s^{-1}, compared to 10 m s^{-1} for LT blades. Considering that races are often won on slender margins, such a speed deficit can be considered enormous. It must be noted that the aerodynamic drag component becomes more dominant at higher speeds. Aerodynamic drag forces are proportional with speed squared, whereas ice friction increases linearly with speed, as indicated by De Koning et al. in Fig. 5b. With speeds in short-track speed skating reaching up to 14 m s^{-1} the impact of ice friction will be lower. Differences in rocker (and bend) radii between short-track skaters are less extreme, however it does reinforce the concern of ice friction in rocker selection. More research with

this method can be used to estimate how much ice friction is currently unknowingly introduced in search of manoeuvrability.

$$\mu F_N v + D v^3 = 1.868 \mu F_N \bar{v} + D \bar{v}^3 \tag{15}$$

B. Low apparent mass

The fit of the force signal to the acceleration of Fig.14 is accurate, however it shows a lower apparent mass than expected. The expected mass is the mass of the sled and skates combined with the ballast, but appears to be lower. This effect gets stronger towards higher values of ballast. A possible explanation for this phenomenon can be found in the frequency response of the load cell. Quick oscillations in speed submit the load cell to sharp force peaks. The load cell may not have enough time to fully settle to the new strain. This would dampen the higher frequency oscillations in acceleration present in the used data, resulting in a flattened slope of the fit.

C. Test method

1) Cross-talk: The test method used has provided clear results and offers good repeatability. The force measurement technique is void of any possible effects of cross-talk. The technique used by De Koning et al. [1] measures deformation of the skate bridge, which is subject to both normal forces and friction forces. De Koning corrects for cross-talk to stay below 0.08%. This is still substantial when considering ice friction to be around 0.5% of the normal force. A second issue arises in the method of De Koning from the angle of the skate with the ice. There is no guarantee that the skate is fully horizontal on the ice. Small angles in the skate relative to the ice can result in a component of the normal force being measured as ice friction. By separating the load cell from the sled in this method, ballast cannot interfere with the ice friction measurement. Additionally, the load cell is guaranteed to be in a horizontal position.

2) Cart: Previous methods found in literature measure the deceleration of a passive slider, as shown in Sec.I-D. The continuous measurement of ice friction was possible in the new method through the use of the cart. The required acceleration feedback is provided by the wheels on the cart. Any friction encountered by the cart has no effect on the force measurement. The position tracking technique was sufficient to correct for d'Alembert forces, as reflected by the quality of the fit in Fig.14. The wheels fitted with rotary encoders provided an uncomplicated and affordable solution. Alternatives such as camera tracking setups or RADAR/LiDAR speed sensors require higher budgets and longer installation times. Tests could be performed in fairly rapid succession, requiring less than 5 minutes for a test run with ballast change, by a single researcher.

3) Flexibility: This method has the added benefit that it does not require any modifications to the skates. Any object can be readily attached to the connection assembly. This makes the method highly adaptable and easy to use for other disciplines (bobsleigh, skeleton, curling, ice hockey). The method can be adapted to test blades at an incline and possibly on a curved trajectory, with extra modifications. Moreover, the method is not limited to ice, but can be used on any flat surface for friction measurements.

D. Limitations

The connection assembly has required several modifications during testing. Setups with flexible connections were trialled for mechanical smoothing of the force signal and added protection of the load-cell. Problems were encountered with unstable oscillations of the sled. Ultimately a rigid connection assembly with a single ball-and-socket joint proved to be effective. This solution required a linear bearing to be added. Time available on the ice for testing was exceedingly limited however during this research, due to COVID-19 related restrictions imposed at Thialf. The staff present at Thialf was put under strain as well, which resulted in difficulties to find time for skate preparations. There were logistical issues due to the weight of the entire measurement setup, which could not remain in the testing area overnight.

The results show a certain level of noise between tests, which may become more problematic when future tests require higher precision to reach statistically significant results. This is partly due to lack of control over external conditions, as it sets a dependency on the ice-rink equipment and maintenance staff. Other sources of noise are the human propulsion, which results in minor irregularities in speed.

V. Conclusion

The impact of rocker on ice friction in short-track speed skating was shown to be substantial.

The large difference in ice friction found between short-track and long-track blades highlights the need for further research. This method was shown to give reliable results with good repeatability between tests. More testing is needed to form a complete picture of the effect of rocker on ice friction. With minor adaptations the method can be applied to test blades at different angles of inclination and on curved trajectories. Ice friction in disciplines such as bobsleigh, skeleton, curling, etc. can be tested by substitution of the sled for objects specific to these disciplines. Due to COVID-19 related restrictions imposed at Thialf in the latter stages of this research, testing time on the ice was limited.

REFERENCES

[1] J. J. de Koning, G. de Groot, and G. J. van Ingen Schenau. Ice friction during speed skating. *Journal of Biomechanics*, 25(6):565–571, 1992.

[2] Anne-Marie Kietzig, Savvas G Hatzikiriakos, and Peter Englezos. Physics of ice friction. *Journal of Applied Physics*, 107(8):4, 2010.

[3] Frank Philip Bowden and David Tabor. The area of contact between stationary and moving surfaces. *Proceedings of the Royal Society of London. Series A. Mathematical and Physical Sciences*, 169(938):391–413, 1939.

[4] Rinse W Liefferink, Feng-Chun Hsia, Bart Weber, and Daniel Bonn. Friction on ice: How temperature, pressure, and speed control the slipperiness of ice. *Physical Review X*, 11(1):011025, 2021.

[5] Edward Lozowski, Krzysztof Szilder, and Sean Maw. A model of ice friction for a speed skate blade. *Sports Engineering*, 16(4):239–253, 2013.

[6] Edward P Lozowski, Krzysztof Szilder, et al. Derivation and new analysis of a hydrodynamic model of speed skate ice friction. *International Journal of Offshore and Polar Engineering*, 23(02), 2013.

[7] Lasse Makkonen and Maria Tikanmäki. Modeling the friction of ice. *Cold Regions Science and Technology*, 102:84–93, 2014.

[8] David CB Evans, John Frederick Nye, and Keith J Cheeseman. The kinetic friction of ice. *Proceedings of the Royal Society of London. A. Mathematical and Physical Sciences*, 347(1651):493–512, 1976.

[9] H Liang, JM Martin, and TL Mogne. Experimental investigation of friction on low-temperature ice. *Acta materialia*, 51(9):2639–2646, 2003.

[10] D Slotfeldt-Ellingsen and L Torgersen. Water on ice; influence on friction. *Journal of Physics D: Applied Physics*, 16(9):1715, 1983.

[11] Frank Philip Bowden and TP Hughes. The mechanism of sliding on ice and snow. *Proceedings of the Royal Society of London. Series A. Mathematical and Physical Sciences*, 172(949):280–298, 1939.